DJS Vol. 48 (2) (2024) – pp. 114-141 ISSN: 1012-5965

Delta Journal of Science
Available online at
https://djs.journals.ekb.eg/

Research Article

GEOLOGY

Geochemistry and Tectonic Evolution of Mélange; A case study of Sikait-Abu Rusheid-Nugrus area of Egyptian Neoproterozoic

Mohamed F. Ghoneim[1]; Mohamed Abu Anbar[1*]; Adel M. Hasan[1]; Mayada A Eldeeb[1]; Ahmed E. Masoud[1,2]

[1] Geology Department, Faculty of Science, Tanta University, Tanta, Egypt
[2] Nanjing Hongchuang Geological Exploration Technology Service Co., Ltd., China

***Corresponding author:** Mohamed Abu Anbar **e-mail:** mmanbar@Science.Tanta.edu.eg

Received: 27/7/2024 **Accepted:** 14/8/2024

KEYWORDS

Sikait-Abu Rusheid-Nugrus shear zone; Mélange; Eastern Desert; Arabian-Nubian Shield; Geochemistry; Tectonic evolution

ABSTRACT

The tectonic mélange of the Sikait-Abu Rusheid-Nugrus area in the Southeastern Desert of Egypt, composed of Proterozoic rock sequences, records a complex history of deformation and magmatism. Despite its significance, the origin and evolution of the studied mélange remain poorly understood due to limited outcrop exposure and structural complexity. This study integrates field observations, petrographic analysis, and whole-rock geochemistry to unravel the provenance and tectonic setting of the Sikait-Abu Rusheid-Nugrus mélange. Petrographic examination reveals a dominant schistose matrix hosting a variety of ultramafic blocks, including serpentinite and ultramafic ortho-schist. Geochemical analysis of major oxides and trace elements indicates that the mélange protolith comprises a mixture of immature wackes, arkoses, and Fe-shales, derived primarily from the erosion of felsic to intermediate igneous sources. The geochemical signatures suggest deposition within an active continental margin setting, further highlighting the dynamic tectonic history of the region. This study provides crucial insights into the geochemistry and tectonic evolution of the Sikait-Abu Rusheid-Nugrus mélange, contributing to a better understanding of the broader tectonic processes and crustal evolution of the Arabian-Nubian Shield.

Introduction

The Sikait-Abu Rusheid-Nugrus area (SAN), located approximately 90 kilometers southwest of Marsa Alam on the Red Sea coast, is a small portion of the Precambrian basement in the southeastern desert of Egypt. It is located in the southeastern section of the Migif Hafafit gneissic complex of the Egyptian Eastern Desert. The complex is an ideal case area to study the exhumation mechanism of high-grade metamorphic rocks **(El-Ramly et al., 1984; El-Bayoumi and Greiling, 1984; Fowler and El-Kalioubi, 2002)**.

The presence of various phases of igneous rocks (i.e., pre-, syn-, and post-tectonic granite) makes the study area one of the best locations in the Arabian-Nubian Shield for studying magma generation as a response to metamorphic and tectonic processes. This area is highly intricate, with psammitic gneisses, mélange rocks, deformed metagabbro, and muscovite garnet granite dominating the landscape **(El-Gaby et al., 1988)**. The mélange consists of a schist matrix and blocks of ultramafic rocks, ophiolitic metagabbro, talc carbonate, orthoschist, and serpentinite. Due to its complexity and unique features, the SAN area within the Arabian-Nubian Shield (ANS) has become a focus of recent research aimed at unraveling its tectonic history and evolution. Mélange, a key component of the SAN area, serves as a crucial tool for understanding this evolution **(El Ramly et al., 1984; Rashawn, 1991, Abu El-Enen et al., 2016)**.

The area chosen for this study is located in the Eastern Desert of Egypt (Fig. 1), particularly in the western part of the Red Sea hills, which is situated in a unique tectonic setting between the Afro-Arabian plate and the Sinai microplate. The area straddles the boundary between the Najd Fault System and the Red Sea. The Najd Fault System is dominated by NE striking sinistral strike-slip faults, inherited from the Pan-African structures and the opening of the Neo-Tethys oceanic basin, which were reactivated and overprinted by a thick sequence of granites and associated volcanic and tectonic events during the Late Proterozoic and Phanerozoic Eons **(Abu-Alam and Stüwe, 2009; Abu-Alam et al., 2014)**. The Red Sea, on the other hand, is a present-day active incipient ocean basin, where the tectonic process and the nature of the associated magmatic and volcanic activities can provide a modern analogue for the evolution of oceanic crust in similar tectonic settings. The study area, called here the "SAN area," is planned to be a key site for a comprehensive study of the nature of evolving tectonic processes and their interaction with magmatism, volcanism, and the development of associated mineralization of the north Red Sea region.

The current study aims to investigate the lithology, geochemistry, and tectonic setting of the Sikait-Abu Rusheid-Nugrus mélange.

This will constrain their tectonomagmatic evolution and provide insight into their metallogenic characteristics. This research will integrate previously published work in the region with current research, thereby improving basic geological knowledge of the area and regional stratigraphic framework. This will be integrated into the wider geotectonic framework of the southernmost Egyptian Eastern Desert to better understand the relationships between the various tectonic blocks and provide constraints on the timing of tectonic events.

Regional Geology and Geologic Setting

The Arabian-Nubian Shield (ANS), a vast Precambrian terrane spanning across Egypt, Sudan, Saudi Arabia, Jordan, and Eritrea, records a protracted history of magmatism, metamorphism, and deformation. The Sikait-Abu Rusheid-Nugrus (SAN) area, located in the ANS, is a significant geological area with a complex tectonic history. This area is characterized by a series of ophiolite complexes, mélanges, magmatic intrusions, and volcanic rocks that were formed during the Neoproterozoic era. The SAN area, which is located in the southeastern sector of the Migif Hafafit gneissic complex, is bounded to the north by the major convex Nugrus thrust **(Greiling et al., 1988; El-Ramly et al., 1993; Fowler and El-Kalioubi, 2002)**. The Hafafit culmination consists of five granitoid-cored domes and is composed of medium-grade metamorphic rocks, including quartzo-feldspathic gneisses and amphibolites. These domes are structurally juxtaposed against overlying supracrustal units along low-angle thrust faults **(Fowler and El Kalioubi., 2002; Kassem et al., 2019)**. The entire Hafafit culmination is further overthrust by an allochthonous ophiolitic mélange, which is exposed extensively to the northeast and east of the study area.

The SAN area forms a prominent, triangle-shaped topographic hill along the major Nugrus Thrust, situated on its hanging wall **(El-Ramly et al., 1984; El-Bayoumi and Greiling, 1984)**. The Nugrus Thrust separates medium-grade metamorphic rocks, including mélange and gneiss of the Hafafit Complex in its hanging wall, from lower-grade metamorphic rocks of the ophiolitic mélange in its footwall (Ghadir area) along Wadi Nugrus and Wadi Sikait **(Greiling et al., 1988; Abd El-Naby and Frisch, 2006)**.

Detailed field studies reveal that metamorphic rocks dominate the exposed rock units, intruded by muscovite-garnet granite. These metamorphic rocks include psammitic gneisses, ophiolitic mélanges, and deformed metagabbros. The ophiolitic mélange, a key unit in the SAN area, is composed of a schistose matrix hosting a variety of blocks, including ultramafic rocks (serpentinite, talc carbonate, talc schist), amphibolite, and metagabbros. Numerous

pegmatite dikes and quartz veins crosscut the metamorphic and igneous units. The SAN area exhibits a high degree of structural complexity, with multiple generations of faults, folds, and joints, generally trending northeast-southwest and northwest-southeast.

Based on field relationships, the following sequence represents the relative ages of the rock units, from oldest to youngest: psammitic gneiss, followed by the ophiolitic mélange (including both its matrix and blocks), then deformed metagabbro, followed by muscovite-garnet granite, then alkali feldspar granite, and finally pegmatite dikes (Fig. 1).

Psammitic gneisses, covering approximately 22.8 km² of the study area, are generally yellowish-brown to pink in color. They are primarily composed of quartz, K-feldspar (including orthoclase, microcline, and perthite), oligoclase, and biotite. Accessory minerals include zircon, thorite, fluorite, apatite, magnetite, hematite, and opaque sulfide minerals. These gneisses are commonly crosscut by intrusions of granite and pegmatite veins.

Field observations and mineralogical compositions permit the categorization of these gneisses into mineralized and barren types. Mineralized psammitic gneisses, primarily located in Wadi Abu Rusheid,

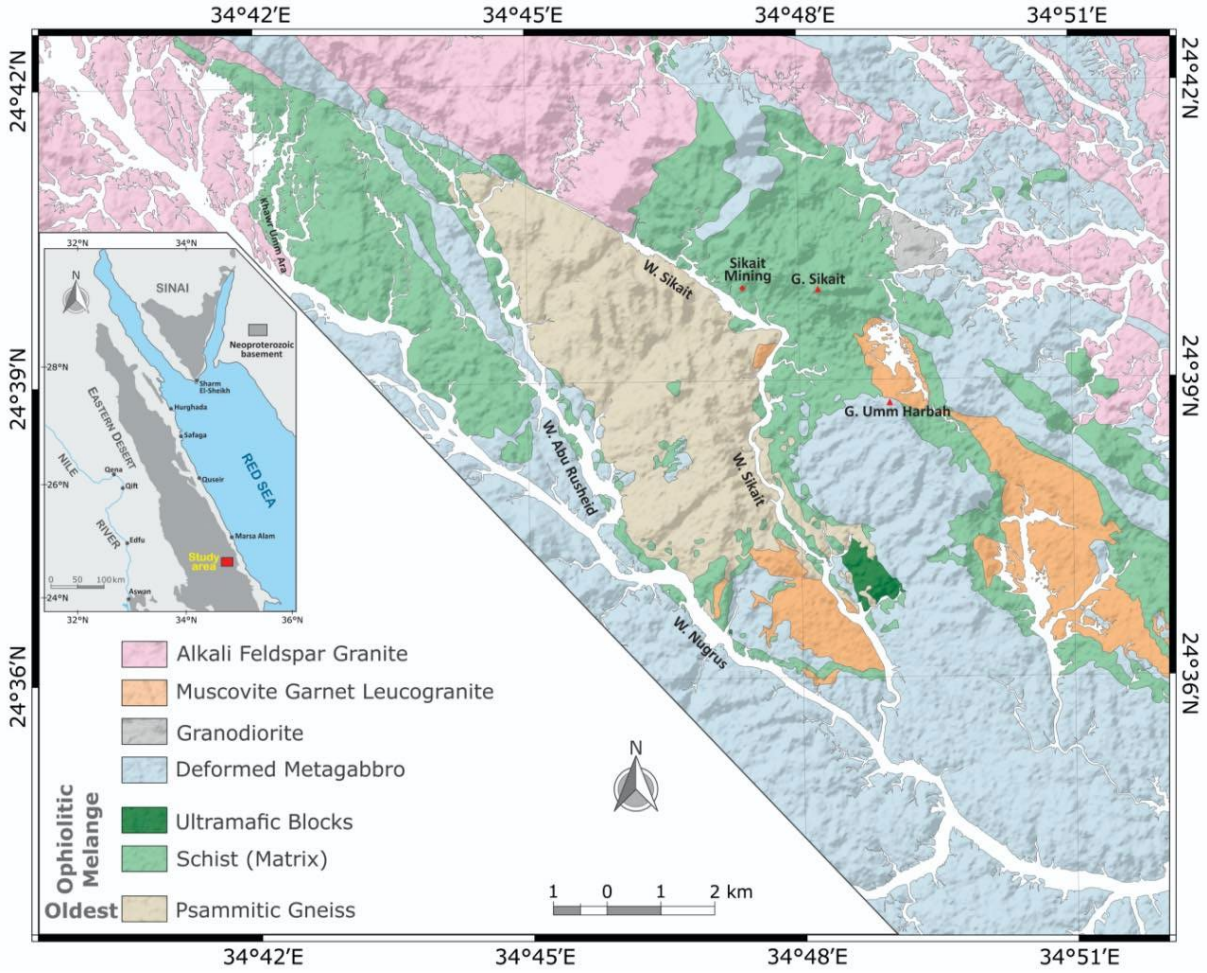

Fig. (1): Geological map of the Sikait-Abu Rusheid-Nugrus area, Southeastern Desert, Egypt.

exhibit a distinctive purple-red color, contrasting sharply with the yellowish-brown to pale pink color of the barren gneisses found in Wadi Sikait. The mineralization is spatially associated with shearing and the emplacement of granite intrusions and pegmatite dikes, particularly along two prominent shear zones trending NNW-SSE and ENE-WSW.

The mineralized gneisses are typically coarse-grained (1-6 mm) and display augen texture (Fig. 2a). Furthermore, radioactive phases are abundant within these gneisses, especially at the mouth of Wadi Abu Rusheid. These gneisses exhibit a well-developed mineral lineation and a preserved bedding plane (S0) that parallels the metamorphic foliation and dips 40°-50°NE. At Wadi Abu Rusheid, the mineralized psammitic gneisses are structurally overlain by the ophiolitic mélange along a thrust fault (Fig. 2b). In contrast, the barren psammitic gneisses are generally medium- to coarse-grained (1-4 mm) and lack the distinctive mineralization and structural complexities observed in their mineralized counterparts. These gneisses often contain enclaves of ophiolitic mélange (Fig. 2c) and are locally intruded by granodiorite in Wadi Sikait (Fig. 2d). In this area, the psammitic gneisses exhibit migmatization along a shear zone and are folded along axes trending N30°W, dipping 40° NE, and N35°W, dipping 70°-80°SW.

The ophiolitic mélange, covering an area of approximately 131.77 km², comprises a schistose matrix hosting a diverse assemblage of blocks, including ultramafic rocks, talc-carbonates, amphibolites, and metagabbros. The mélange exhibits strong foliation, characterized by folded and boudinaged pegmatite veins aligned parallel to foliation planes. Schist is the dominant lithology in the mélange matrix, with variations including garnet-rich schist, amphibolite schist, and quartzo-feldspathic schist. In Wadi Nugrus, schist, covering an area of about 76 km², is structurally thrust over deformed metagabbro and is influenced by a NW-SE trending shear zone (Fig. 2e). Similarly, in Wadi Abu Rusheid, schist overlies psammitic gneiss along a thrust fault and forms anticlinal folds with axial planes parallel to the direction of Wadi Abu Rusheid. Along the southern tributary of Wadi Abu Rusheid, schist occurs as enclaves within the psammitic gneiss. Amphibolite rocks in the mélange are intruded by muscovite garnet granite, which exhibits a westward tilt. Additionally, amphibolite occurs as folds with a fold axis trending N65°W and dipping 67° NW. The schist in these regions displays intense shearing, characterized by an eastward foliation direction and a composition dominated by talc, graphite, garnetiferous biotite, and amphibolite schist.

Fig. (2): Field photographs of key lithological and structural relationships in the Sikait-Abu Rusheid-Nugrus area. (a) Augen texture in psammitic gneiss, displaying a well-developed gneissose fabric. (b) A normal fault juxtaposing mélange against psammitic gneiss, with the mélange thrust over the gneiss along a later structure. (c) Enclaves of ophiolitic mélange thrust in psammitic gneiss. (d) Granodiorite intrusion crosscutting psammitic gneiss. (e) Schist overthrust by deformed metagabbro along a thrust fault. (f) Northeast-trending foliation in schist, oriented perpendicular to the Nugrus shear zone. Legend: M = Mélange, Gn = Gneisses, Gr = Granite.

Ultramafic blocks, primarily composed of serpentinite, are prominent features within the SAN area, ranging in size from small boulders to large (about 20 m) blocks. These blocks are particularly well-exposed in Wadi Nugrus, Wadi Sikait, and Wadi Abu

Rusheid. In Wadi Nugrus, serpentinite is structurally juxtaposed atop both ophiolitic metagabbro and mélange along thrust faults. Specifically, serpentinite overlies meta-gabbro along ENE-WSW trending faults dipping 280°/NNW and mélange along NW-SE trending faults dipping 37°/NE. Notably, within an area intruded by muscovite-garnet granite, an ultramafic dyke cuts through an ultramafic block, which may be classified as wehrlite (Fig. 3d). The Wadi Sikait tributary has ultramafic fragments obducted in schist. These fragments primarily consist of serpentinite, ultramafic ortho-schist, and talc carbonate. Ultramafic ortho-schist with talc carbonate contacts schist at the shear zone. The ultramafic rocks display a range of colors, including black, yellowish-green, and crimson. Some black to brown minerals, tentatively identified as ankerite, are 1-7 cm in diameter and occur within talc carbonate serpentinite.

Wadi Sikait exhibits evidence of significant deformation, including a granite dyke-like body intruding schist and deformed metagabbro. Left-lateral displacement towards the east is indicated by slickensides observed within the Wadi. Schists display striations trending N 55°W and dipping 80° NE, aligning parallel to the Nugrus shear zone. Notably, numerous folds within Wadi Sikait tributaries also trend parallel to the Nugrus shear zone. This deformation is further evidenced by a quartz vein folded and faulted parallel to the Nugrus shear zone (NW-SE trend) at the contact between schist and metagabbro (Fig. 2e). The schist itself exhibits a northeast foliation perpendicular to the Nugrus shear zone (Fig. 2f). Furthermore, granitic and pegmatite dikes intrude the schist, displaying orientations both parallel to Wadi Nugrus (Fig. 3a) and perpendicular to the shear zone (Fig. 3b).

Deformed metagabbro covers a significant area of approximately 63 km² and forms fold-thrust sheets across Wadi Sikait, Wadi Nugrus, and Wadi Abu Rusheid. It exhibits a NW-SE trending foliation and dips 330°/NE. In Wadi Sikait, deformed metagabbro and granite are thrust over schist, trending N35°W and dipping 45° E. This metagabbro is intruded and crosscut by folded deformed pegmatite, trending N15°W and dips eastward in Wadi Nugrus and is faulted along a NW-SE trending plane. Slickensides in the deformed metagabbro at Wadi Abu Rusheid indicate NW-SE oriented movement (Fig. 3e). Granitic offshoots within the metagabbro create irregular or dike-like bodies parallel to foliation planes. In Wadi Sikait, the metagabbro displays deformation, foliated NW-SE and dipping 45°NE, thrusted by mélange, and intruded by a granitic vein. The intensity of deformation increases westward, culminating in upper amphibolite facies metamorphism and migmatization.

Muscovite garnet granite occurs in Wadi Nugrus, Sikait, and Abu Rusheid,

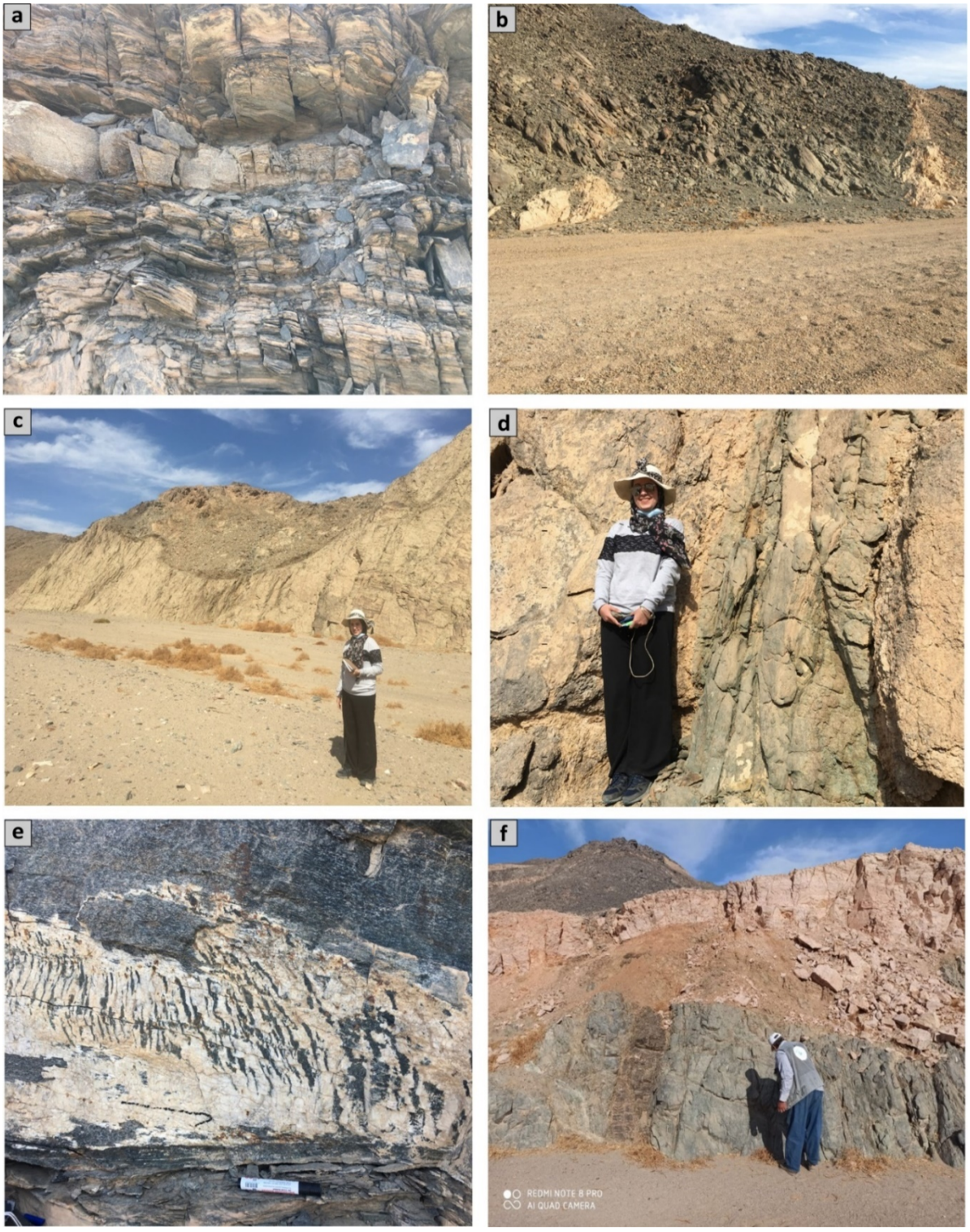

Fig. (3): Field photographs showing structural relationships within various lithological units in the Sikait-Abu Rusheid-Nugrus area. (a) Granitic and pegmatitic dikes intruding schist parallel to Wadi Nugrus. (b) Granitic and pegmatitic dikes intruding schist perpendicular to the shear zone. (c) Ultramafic blocks enclosed within schist. (d) An ultramafic dike crosscutting an ultramafic block, potentially representing wehrlite. (e) Slickensides on a fault surface within gneissose metagabbro, indicating NW-SE directed shear, Wadi Abu Rusheid. (f) Deformed pegmatite dike intruding and crosscutting metagabbro.

covering an area of about 10 km². In Wadi Nugrus, granite is pegmatitic and occasionally contains tourmaline, beryl, and garnet. It displays a white color (sometimes reddish) and varies in grain size from fine to coarse. Granite intrusions in the mélange are

characterized by faulting, folding, and a NW-SE trend. In Wadi Abu Rusheid, some granitic dikes align with the main wadi trend, while others occur as dike-like bodies at the entrance of Wadi Sikait, trending NW parallel to the Nugrus shear zone. These granitic dikes exhibit deformation and shearing, containing mica and garnet. A distinct type of granite, characterized by a lack of deformation, intrudes both the mélange and gneisses. In the northern part of Wadi Sikait, the granite is highly deformed and sheared at its contact with the mélange, with apophyses intruding into the gneisses.

Alkali feldspar granite outcrops at the end of Wadi Sikait and Wadi Abu Rusheid, forming high, pink mountains. These mountains exhibit shearing along the Sikait shear zone, indicating significant deformation. In the northern part of the study area, granite intrudes both psammitic gneiss and mélange.

White to beige pegmatite dikes (Fig. 3f), characterized by very coarse to coarse grain sizes, are observed across various regions, including Wadi Nugrus and Wadi Abu Rusheid. These dikes trend N-S, paralleling schist foliation planes and occasionally displaying boudinage structures within the mélange.

Petrography

Psammitic Gneisses

Two distinct types of psammitic gneisses have been identified based on field observations and mineralogical compositions:

a. Mineralized psammitic gneiss

This medium-grained gneiss is characterized by a mineral assemblage dominated by quartz, plagioclase, alkali feldspar, and muscovite. It is notably enriched in radioactive minerals, including zircon, fluorite, thorite, and uranium minerals such as kasolite and columbite (Fig. 4a). Mylonites exhibiting cataclastic textures are frequently observed along thrust zones. Large aggregates or streaks of coarse quartz with sutured margins often host rows of minute prismatic zircon crystals. Quartz constitutes the principal component, occurring as porphyroblasts or anhedral aggregates. Some plagioclase crystals display zoning, while alkali feldspars predominantly comprise perthitic microcline and orthoclase. Muscovite, which may contain plagioclase inclusions, occurs in two distinct orientations: parallel to the main foliation planes and perpendicular to them. Zircon, occasionally metamict, ranges in size from medium to coarse (0.2 to 0.3 mm). Minor amounts of anhedral fluorite are present, likely due to its mobility during deformation. Columbite occurs as minute crystals, while iron oxides exhibit deformation and cataclastic textures. Uranophane (U) is found to be adsorbed onto iron oxides, and reddish-brown metamict thorite is isomorphous.

b. Barren psammitic gneiss

This medium- to coarse-grained gneiss displays gneissose textures and augen structures, predominantly quartzo-feldspathic in composition. The mineral

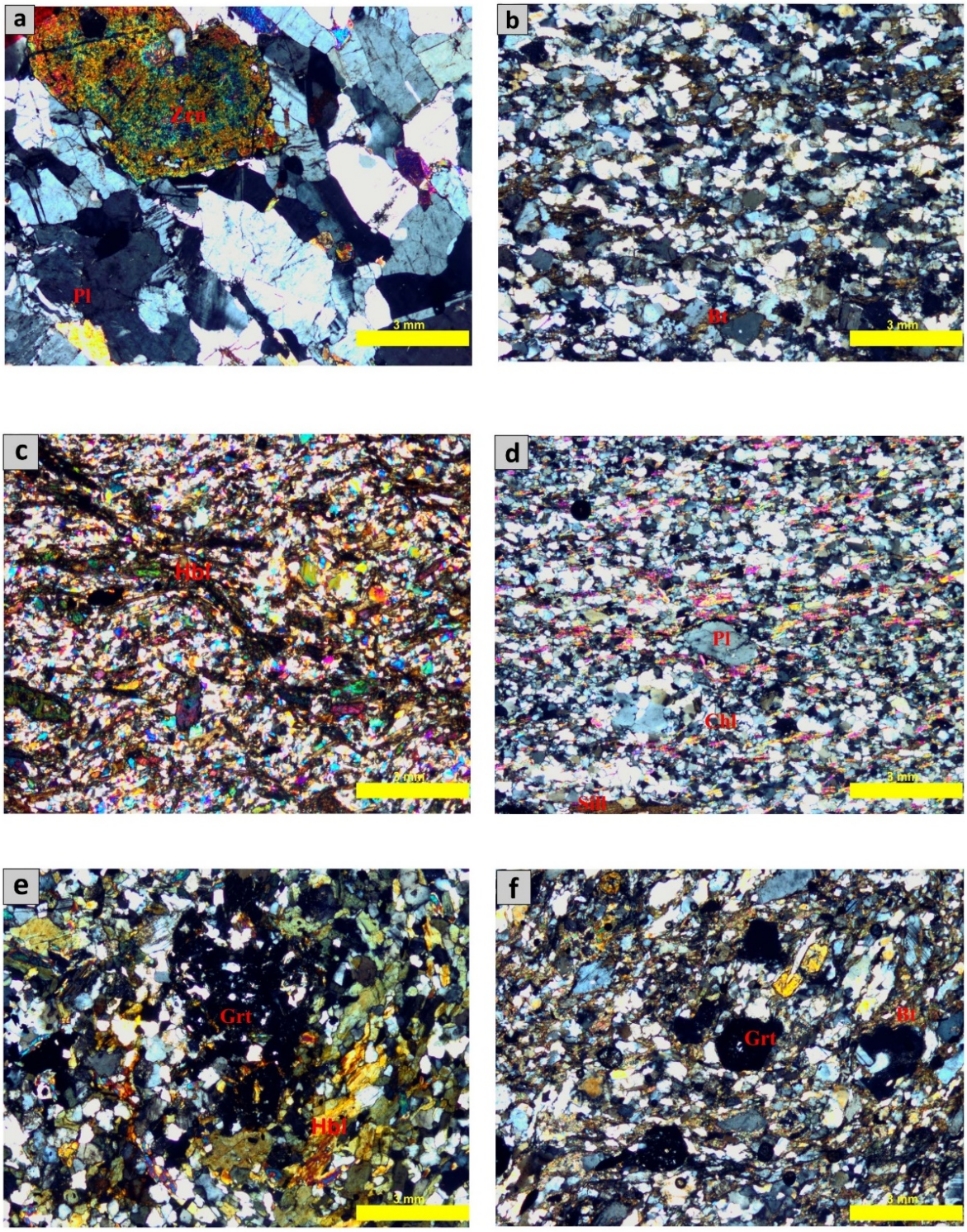

Fig. (4): Representative photomicrographs (CPL) of key lithologies from the Sikait-Abu Rusheid-Nugrus area. (a) Mineralized psammitic gneiss. (b) Barren psammitic gneiss. (c) Biotite-muscovite schist. (d) Chlorite-muscovite schist. (e) Garnet-amphibolite schist. (f) Quartzo-feldspathic schist.

assemblage is dominated by quartz, plagioclase, potash feldspars (orthoclase, microcline, and perthite), and biotite, in decreasing order of abundance. Alkali amphiboles, such as arfvedsonite and riebeckite, are also present. Accessory minerals include zircon, allanite, and opaque or iron oxide minerals (Fig. 4b). Quartz forms xenoblastic interlocking crystals in a granoblastic texture, occasionally exhibiting

elongation. Feldspar, comprising approximately 30% of the rock, occurs as xenomorphic aggregates and porphyroblasts, displaying weak deformation characterized by displaced, bent, and sometimes rotated twin lamellae. The anorthite content of plagioclase ranges from 15–35%, reflecting a composition ranging from oligoclase to andesine. Reddish-brown biotite flakes intergrown with alkali amphiboles exhibit a preferred orientation around feldspar porphyroblasts. Arfvedsonite and riebeckite interact with secondary iron oxides, forming platy crystal aggregates and thin streaks arranged parallel to plagioclase and augen potash feldspar. Subhedral grains and clusters of opaque minerals, such as magnetite and hematite, also display a preferred orientation. Colorless to pale brown subhedral to euhedral idioblastic and porphyroblastic garnet crystals are present, along with muscovite.

Ophiolitic Mélange

The ophiolitic mélange is characterized by a schistose matrix hosting a diverse assemblage of blocks, including ultramafic rocks, talc-carbonates, amphibolites, and metagabbros.

Schistose matrix

a. Biotite muscovite schist

This schist is the most prevalent schist type in the area, appearing as a compact, yellowish rock. Its mineral assemblage is dominated by quartz, plagioclase, biotite, and muscovite (Fig. 4c). Magnetite and rutile occur as accessory minerals, while chlorite is the primary secondary mineral. Biotite, the dominant mineral, appears as long, dark brown grains exhibiting strong pleochroism. These grains are embedded within quartz crystals and form flaky, acicular, and patchy crystals up to 0.15 mm in size. They typically display a fine to medium grain size and are predominantly sub-parallel to the main schistosity. Biotite rims often exhibit alteration to chlorite and corrosion by quartz. Muscovite forms colorless, acicular, flaky crystals up to 0.2 mm, frequently occurring as solitary fine-grained crystals within the groundmass. "Mica fish" shapes are common in sheared muscovite grains, sometimes forming thick clusters and bands intercalated with chlorite crystals and fine-grained quartz. Chlorite appears as pale green patches, irregular flaky crystals, and rarely elongate idiomorphic crystals up to 0.1 mm within the groundmass. It forms dense clusters and patches intercalated with muscovite crystals, defining schistosity, or as a secondary mineral from partially altered biotite flakes. Garnet crystals occur as medium-sized idioblasts reaching up to 0.3 mm. Quartz forms medium to fine anhedral crystals, parallel to the foliation, up to 0.12 x 0.06 mm, exhibiting wavy extinction and typically sutured and corroded rims. It is usually elongated and crushed, parallel to the major schistosity. Mostly parallel quartz

grains alternate with biotite and muscovite to create a schistose texture. Plagioclase (An_{35}) is rare, appearing as short tabular crystals of medium size (0.1 to 0.3 mm), highly corroded, sericitized, and rarely twinned. Magnetite crystals are dark-colored, euhedral, medium-sized up to 0.2 mm, irregular, and widely distributed in the groundmass. Small opaque and quartz crystals are aligned and contained within magnetite.

b. Chlorite muscovite schist

It is characterized by a mineral assemblage dominated by quartz, plagioclase, hornblende, muscovite, and chlorite, in decreasing order of abundance. Iron oxides are the main accessory mineral (Fig. 4d). The main schistosity is defined by chlorite intercalating with quartz, feldspars, and hornblende as pale to dark green acicular and minute elongated streaks in the groundmass. Muscovite appears as colorless fine-grained elongate streaks with chlorite, showing intense interference colors. Most chlorite forms parallel clusters or bands, with isolated crystals up to 0.1 mm long. Sheared, wavy-extinction quartz crystals range from 0.1–0.15 mm in size. Muscovite and chlorite surround lensoidal clusters, with parallel quartz clusters running along the main schistosity. Rare idiomorphic short tabular plagioclase crystals up to 0.2 mm are present, often distorted and corroded by quartz, with lamellar twinning. Quartz and fine muscovite streaks are common within plagioclase crystals, which sometimes exhibit fish shapes.

c. Garnet amphibolite schist

This schist type forms extensive belts along the E-W axis in the southern part of the research area. Hand specimens are green with pronounced schistosity. The primary minerals are quartz, plagioclase, and hornblende, with chlorite, epidote, and calcite as secondary minerals. Garnet and iron oxides are the main accessory minerals (Fig. 4e). This unit resembles biotite hornblende schist but includes garnet porphyroblasts in a matrix mainly of biotite, hornblende, and quartz, indicating medium to high-grade metamorphism. Garnet forms idioblastic crystals up to 0.5 x 0.5 mm, with both euhedral and subhedral varieties. In the matrix, garnet crystals create a porphyroblastic texture, with quartz and feldspar also present. Iron oxides form 0.1-mm crystals. They are often idiomorphic crystals widely distributed in the groundmass or surrounded by hornblende. Few fine-grained quartz crystals, up to 0.1 mm, are found, typically parallel to the schistosity, forming clusters of highly sheared and ground crystals mixed with groundmass elements. Quartz can be surrounded by hornblende or grow along schistosity with rims and may combine with groundmass components. Porphyroblasts with extended ends and an augen texture show undulose extinction and quartz vein infiltration. Plagioclase (An_{35-40}) crystals are

colorless, short tabular, and range from xenomorphic to idiomorphic, with lamellar twinning and sizes of 0.1-0.2 mm. Some are bordered by chlorite and corroded by quartz. The long axis of plagioclase is sub-parallel to the schistosity. Hornblende crystals are stretched, xenomorphic, and pale green, with sizes up to 0.25 mm and an angled cleavage. Most hornblende crystals are corroded by quartz and plagioclase, sometimes with chloritized rims and significant distortion. Crystals are quartz-rich and opaque, sub-parallel to the schistosity, with varying degrees of deformation. Biotite forms fine to medium flakes and plates (0.2 mm) that align parallel to the schistose texture, alongside quartz and hornblende in the matrix.

d. Quartzo-feldspathic schist

This schist type is characterized by pale green, compact rocks. Plagioclase (albite), quartz, biotite, and muscovite dominate, while orthoclase is negligible. Secondary minerals include epidote and chlorite, with iron oxides and zircon as accessories (Fig. 4f). Albite (An_{15}) forms medium to coarse porphyroblastic crystals up to 0.2 mm, with idiomorphic morphologies ranging from equant to short prismatic. Albite contains scattered muscovite, quartz, and chlorite. Quartz crystals, fine to medium and up to 0.1 mm, are characterized by eroded edges and wavy extinction. They are either distributed throughout the groundmass or confined by albite. Biotite is pleochroic from pale to dark brown, forming bands parallel to the matrix, with a schistose texture, sometimes folded. Muscovite occurs in chlorite intercalations or thick albite bands, appearing as fine-grained, needle-like crystals up to 0.2 mm with high interference colors. Iron oxides are dark grains up to 0.05 mm, uniformly scattered in the groundmass. Chlorite forms medium-sized subhedral to anhedral crystals, pale green, flaky, patchy, and acicular. They intercalate with muscovite crystals to define the major schistosity. Epidote crystals range from colorless to pale yellow to green, typically irregular, but sometimes equant and idiomorphic, with fine to medium sizes up to 0.1 mm. Epidote occurs parallel to the primary schistosity.

Ultramafic blocks

a. Serpentinite

It occurs as sheared, massive blocks displaying a range of colors, including dark grey, greyish-green, green, and yellowish green. This fine-grained rock is predominantly composed of serpentine minerals such as antigorite, chrysotile, magnesite, and chromite, with minor talc, ankerite, calcite, and magnetite (Fig. 5a).

Antigorite forms anhedral flakes exhibiting radial distribution, occasionally forming fibro-lamellar aggregates up to 0.85 mm long, arranged sub-parallel in a decussate pattern. Antigorite crystal aggregates can display mesh and bastite textures. Some serpentinite samples exhibit

shearing due to the parallel alignment of antigorite.

Chrysotile appears as dispersed grains or uneven plates, often displaying black-bloody red coloration indicative of transformation to talc. Iron oxides occur as anhedral patches or veins, with euhedral to subhedral crystals reaching up to 1.25 x 1.37 mm in some samples. Magnesite occurs as large uneven patches, occasional grains, and colorless veinlets. Talc, exhibiting high interference color, is present in small amounts alongside serpentine minerals. Chromite occurs as subhedral to anhedral crystals ranging in size from 0.6 x 0.52 mm to 1.5 x 0.85 mm. Euhedral and subhedral idioblastic ankerite crystals up to 0.2 x 0.5 mm are also present, appearing pale brown in plane polarized light (PPL) and black in CN. Ankerite crystals, embedded within serpentine, create a porphyroblastic texture, often distorted and degrading to talc. Some samples contain quartz veins up to 0.12 x 0.25 mm or dispersed anhedral crystals.

b. Talc carbonate serpentinite

These rocks are characterized by significant carbonatization, where antigorite is replaced by carbonate minerals. This fine-grained, silky rock exhibits a buff to light creamy color and a soapy texture. Serpentine minerals (primarily antigorite) constitute approximately 50% of the rock, forming radial, flaky, and fibro-lamellar structures. Large plates up to 0.5 mm across may form from tiny flakes or exhibit flame habits. Talc, second in abundance to serpentine, appears ultra-white with strong interference color. The rock displays uneven grains, with talc occurring in small amounts as tiny fibers between carbonate minerals. Fine to medium-sized veins or patches of carbonate minerals are also present. Chromite appears reddish-brown in PPL and dark red in CN, with a grain size of 0.65 x 0.5 mm and cracks, exhibiting uneven grain distribution. Iron oxides are distributed among carbonates and serpentine minerals.

Deformed Metagabbro

This rock is predominantly represented by hornblende gabbro and exhibits a hypidiomorphic, ophitic, and subophitic texture (Fig. 5d). It is composed primarily of plagioclase, amphibole, biotite, quartz, and minor potash feldspar. Accessory minerals include iron oxides, sphene, and zircon. Epidote, sericite, and chlorite occur as secondary minerals. Plagioclase, with an andesine composition (An_{45-50}), displays a blasto-ophitic texture intergrown with hornblende, constituting approximately 45.4% of the rock. It frequently contains inclusions of hornblende, quartz, and zircon.

Quartz forms fine subhedral grains up to 0.05 mm, often included within plagioclase, exhibiting clear crystals with occasional wavy extinction. Hornblende, the primary mafic mineral, occurs as twinned euhedral to subhedral crystals up to 1.3 mm, displaying two cleavage sets and strong pleochroism ranging from pale green to green. It often

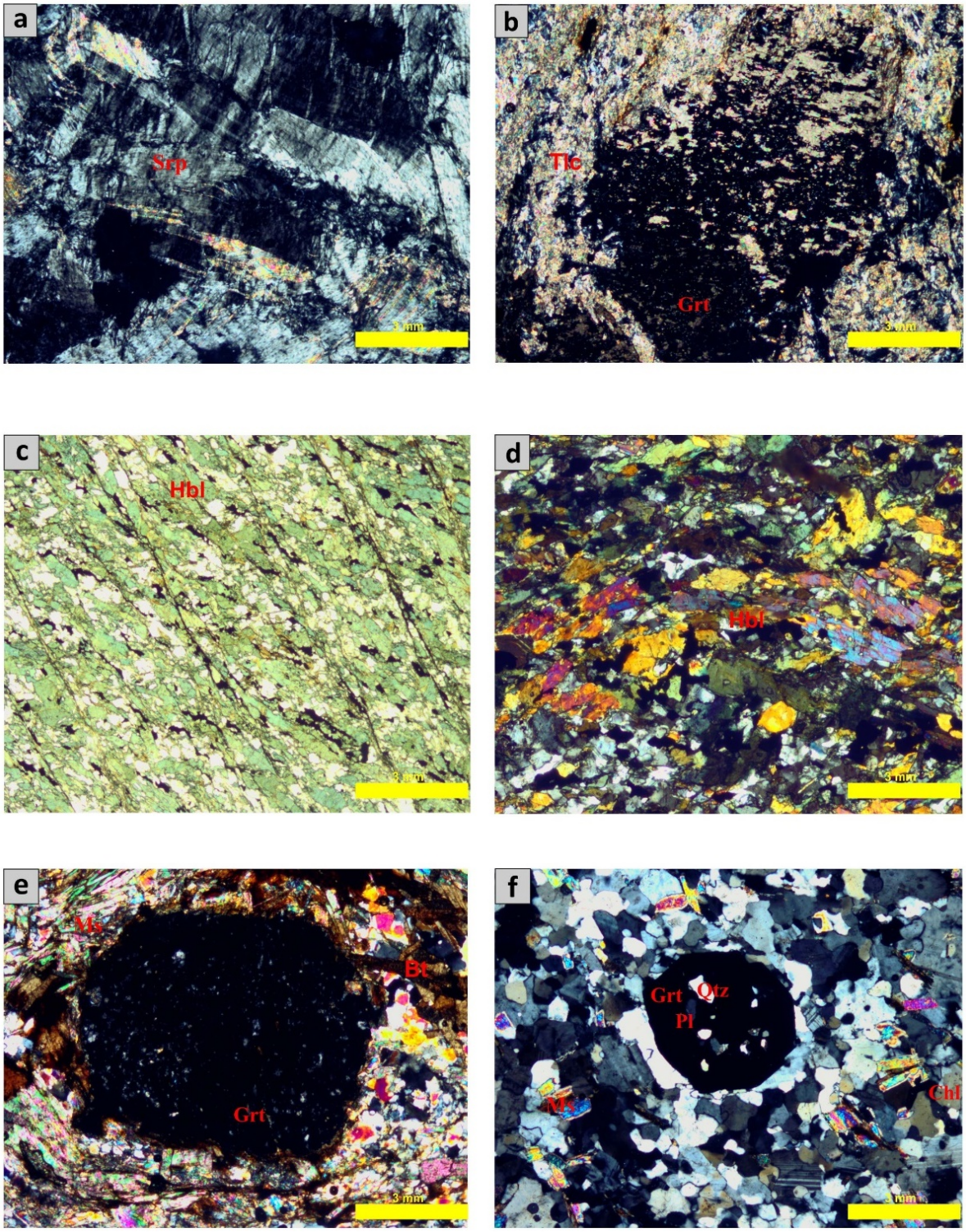

Fig. (5): Representative photomicrographs (CPL) of key lithologies from the Sikait-Abu Rusheid-Nugrus area. (a) Serpentinite. (b) Talc-carbonate serpentinite. (c) Gneissose metagabbro. (d) Highly altered plagioclase exhibiting blasto-ophitic texture with hornblende. (e) Deformed granite. (f) Undeformed granite.

contains inclusions of epidote, quartz, and zircon and is frequently invaded by biotite. Actinolite, a secondary mineral, forms sub-idiomorphic asbestiform prisms up to 2 x 0.9 mm, scattered within plagioclase. It is colorless to pale green with faint pleochroism. Tremolite, occasionally present, is colorless to pale green. Hornblende exhibits two distinct orientations associated with iron oxides,

indicating different deformation phases and folding. Sericite, a product of plagioclase alteration, appears as colorless, acicular crystals. Chlorite occurs as fine flakes and irregular grains of pale green, displaying brown and deep gray interference colors. It is associated with tremolite and plagioclase (0.3 to 1 mm), often forming after hornblende alteration Sphene, associated with iron oxides, appears as thin films or rhombic crystals, scattered within plagioclase and hornblende (0.15 to 0.2 mm), and sometimes as fish-like bodies. Epidote forms aggregates with high-order interference colors within plagioclase crystals and patches within plagioclase and amphibole (0.1 to 0.3 mm).

Deformed Muscovite Garnet Granite

This rock appears white to whitish grey and is mainly composed of quartz, potash feldspars, plagioclase, muscovite, garnet, and a small amount of biotite. Zircon, allanite, sphene, apatite, and iron oxide are accessory minerals, while sericite and chlorite are secondary (Fig. 5e). Thin sections show folding and bending, with foliation in country rock compressing finer quartz crystals into thin bands and causing undulose extinction and serrated sub-grain boundaries. Plagioclase (An10-20) lamellae bend due to twinning and deformation. Potash feldspar crystals are often deformed and filled with quartz and muscovite. Microcline and orthoclase have perthitic intergrowths. The rock has myrmekite between quartz and potash feldspar due to deformation, recrystallizing into fine grained aggregates. Muscovite is found near garnet borders and transforms into chlorite and iron oxides, showing cataclastic effects and folding. Deformed biotite can become muscovite, forming pale brown to dark brown subhedral crystals. Quartz, plagioclase, muscovite, iron oxide, chlorite, and biotite are present in garnet, which has a corona texture and brittle breakage parallel to groundmass foliation. The garnet corona has muscovite on the exterior and biotite on the interior, with printed chlorite over muscovite. Minerals are absent from the garnet's periphery, indicating garnet evolved in two phases: inclusion and a mineral-free zone. Zircon prisms are surrounded by quartz and muscovite, with some crystals showing concentric color zones and metamict features. Opaques are tiny subhedral grains and anhedral interstitial skeletal crystals.

Non-deformed Muscovite Garnet Granite

It is medium to coarse-grained, mainly consisting of potash feldspar, plagioclase, quartz, and biotite, with less hornblende. Accessory minerals include zircon, fluorite, allanite, apatite, sphene, and opaque minerals, while secondary minerals are chlorite, muscovite, and kaolinite (Fig. 5f).

Potash feldspar forms euhedral or aggregates with perthitic and myrmekitic textures, generally corroded by biotite and quartz. Perthites are patchy and flame-like,

and they, along with quartz, corrode microcline, forming subhedral crystals. Plagioclase (An10-20) is sometimes corroded by string perthite, showing albite twinning.

Quartz forms subhedral to anhedral crystals in interstitial gaps or corrodes plagioclase, perthite, and biotite, showing graphic texture and wavy extinction. Anhedral to subhedral biotite flakes are dark brown to yellowish-brown, sometimes transforming into muscovite.

Yellowish to reddish-brown garnet forms large euhedral to subhedral grains ranging from 0.4 to 5 mm, containing quartz, plagioclase, and chlorite. Zircon, characterized by an iron oxide ring, great relief, and colorlessness, can exhibit fractures, metamictization, and pleochroic halos due to radioactive inclusions. Chlorite forms irregular pale greenish granules with abnormal interference colors as a secondary alteration product of biotite. Sericite is a product of potash feldspar's altered edges and crystal cleavage.

Methodology

Whole-rock geochemical analyses of mélange samples were performed for major, trace, and rare earth elements. Analyses were conducted at the Ferrara University laboratories in Italy using an ARL Advent–XP spectrometer and the full matrix correction method of **Lachance and Trail (1966)**.

Results

Whole Rock Geochemistry

The mélange is classified based on grain size and chemical composition (Table 1). Geochemical analyses reveal a SiO_2 content ranging from 49.7 to 73.2 wt%, with Al_2O_3 exhibiting a narrower range of 12.7-14.1 wt%. TiO_2 content is relatively high, ranging from 0.2 to 1.4 wt%. Notably, the mélange displays elevated CaO (0.9-8.3 wt%), Na_2O (1.9-5.6 wt%), and Fe_2O_3 (3.2-9.9 wt%) abundances, but lower K_2O (1.6-3.95 wt%) abundances (Fig. 6).

Trace element concentrations (ppm) are also variable, with Zr ranging from 175 to 482, Zn from 175.7 to 482.6, Th from 3.5 to 12.7, and V from 9.9 to 226.2. Other notable trace elements include Ga (14.4-28.2), Hf (1.7-20.1), La (12.1-90.2), Mo (1.7-7.6), Nd (17.5-95.7), Ni (2-103.9), Pb (9.9-21.9), Y (21.4-115), Rb (24.2-90), Sr (62.2-422.6), Co (3-43.7), Cr (1.7-460.7), Ce (31.9-194), and Ba (222.7-641.1) (Figs. 7, 8, and 9).

Chondrite-normalized trace element patterns **(McDonough and Sun, 1995)** (Fig. 10a) reveal enrichment in Cr, Ni, Ga, Rb, Sr, Y, Zr, Ba, and Pb, while exhibiting depletion in Co, Cu, Zn, Mo, Cs, La, Ce, Pr, Nd, Hf, W, Th, U, and Zr. In contrast, upper continental crust-normalized trace element patterns **(Taylor and McLennan, 1995)** (Fig. 10b) indicate enrichment in Y, Zr, Mo, Nb, Cs, and W, with depletion in V, Cr, Ni, Cu, Rb, Sr, Ba, Pb, Th, and U (Supplementary 1).

Table (1): Geochemical Analysis of Mélange from the Sikait-Abu Rusheid-Nugrus area.

Rock unit	mélange					
Sample No.	67M	68M4	68M5	69Mc	70Mc	72M2
SiO_2	67.068	71.823	70.976	73.408	49.726	71.082
Al_2O_3	13.93	14.166	13.9	12.704	14.392	13.377
Fe_2O_3	5.288	3.236	3.549	3.433	9.934	3.444
MnO	0.082	0.055	0.052	0.056	0.148	0.048
MgO	1.7	0.48	0.454	0.163	8.531	1.087
CaO	3.835	0.901	1.105	0.386	8.34	2.172
Na_2O	3.757	5.606	5.442	3.824	1.898	3.974
K_2O	1.563	1.816	2.299	3.95	1.815	2.435
TiO_2	0.728	0.27	0.325	0.205	1.487	0.525
P_2O_5	0.118	0.027	0.044	0.021	0.735	0.074
LOI	0.76	0.39	0.53	0.33	0.93	0.42
Sum	98.93	98.93	98.9	98.67	98.19	98.78
Trace elements (ppm)						
Ba	222.7	239.4	882.6	641.1	559.5	339.7
Ce	34.9	125	137.6	194	55.7	31.9
Co	15.3	3.5	5.5	3	43.7	9.8
Cr	4.6	0	1.7	0	460.7	5.9
Cs	10.8	3.9	0	0	19	9.7
Cu	43.7	19.8	0.5	1.1	26.6	222.8
Ga	14.4	18.3	28.2	20.3	19.2	15.6
Hf	5.9	20.1	15.1	14.8	1.7	10.8
La	12.1	65.1	66.8	90.2	37.2	29.7
Mo	1.7	7.6	6.1	4.6	2.1	2.6
Nb	0	23.9	28.4	20.1	0	0
Nd	30	86.8	81.2	95.7	35.1	17.5
Ni	12.1	5.6	5.4	2	103.9	4.8
Pb	9.9	11.5	21.9	14	7.5	12.1
Pr	0	10.7	19	30.1	14.7	3.3
Rb	47.5	24.2	41.3	69	90.8	51.2
Sc	12.8	0	9.7	6.4	22.5	0
Sr	161	138.1	133.4	62.2	422.6	196.1
Th	3.5	6.9	8.8	10.4	4.5	12.7
U	0	3	0.2	1.6	0	0
V	83.4	9.9	20.9	7.4	226.2	73.2
W	28.1	42.8	32.9	42.1	30.7	36.1
Y	33.3	113.5	107.6	83.1	21.4	27.1
Zn	59.5	106.7	152.2	80.1	88	40.6
Zr	175.7	482.6	424.5	425.9	208.1	212.4

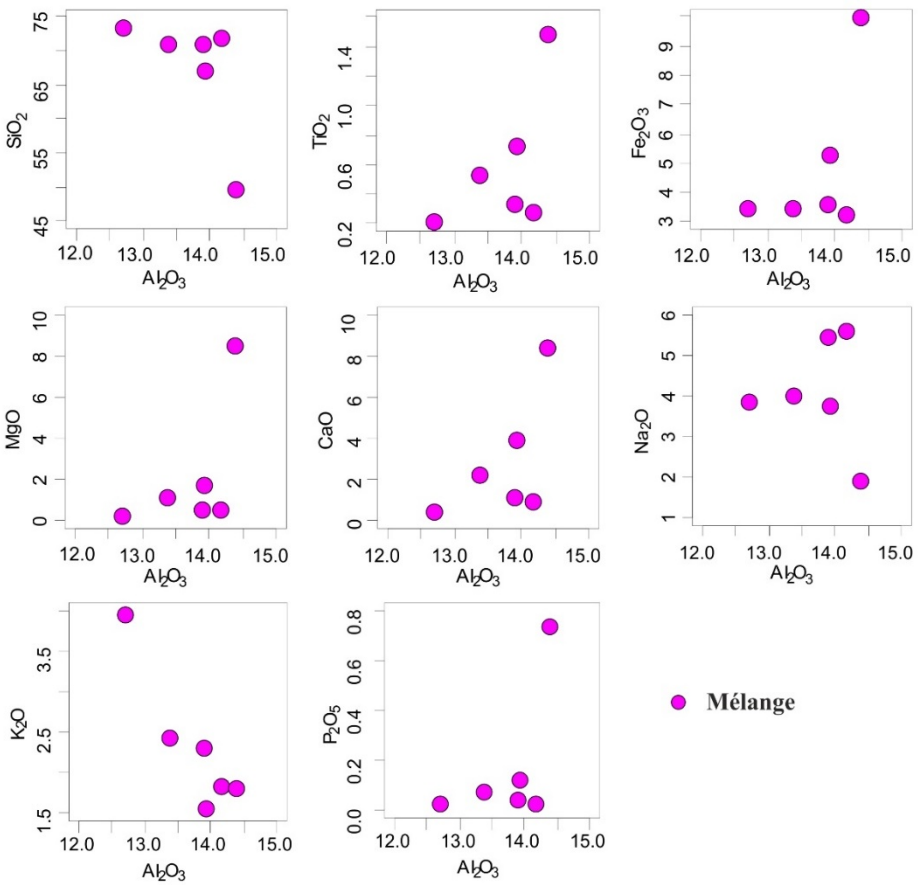

Fig. (6): Multi-elemental variation diagrams of major oxides versus Al_2O_3 (wt. %) for the studied mélange.

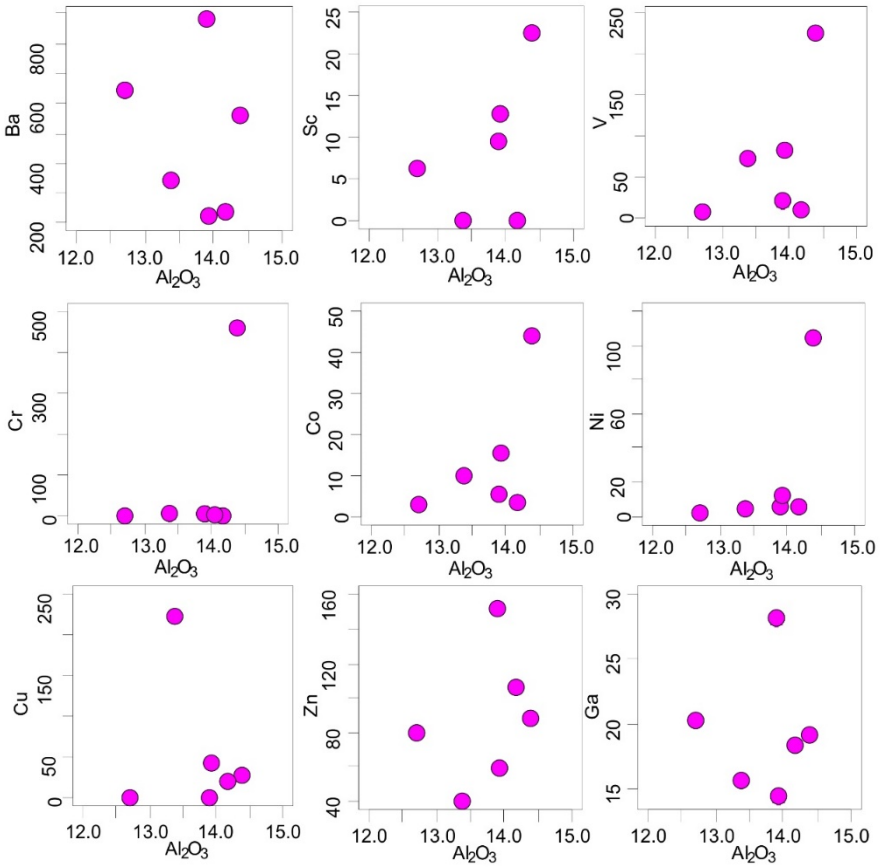

Fig. (7): Multi-elemental variation diagrams of some trace elements (ppm) versus Al_2O_3 (wt. %) for the studied mélange.

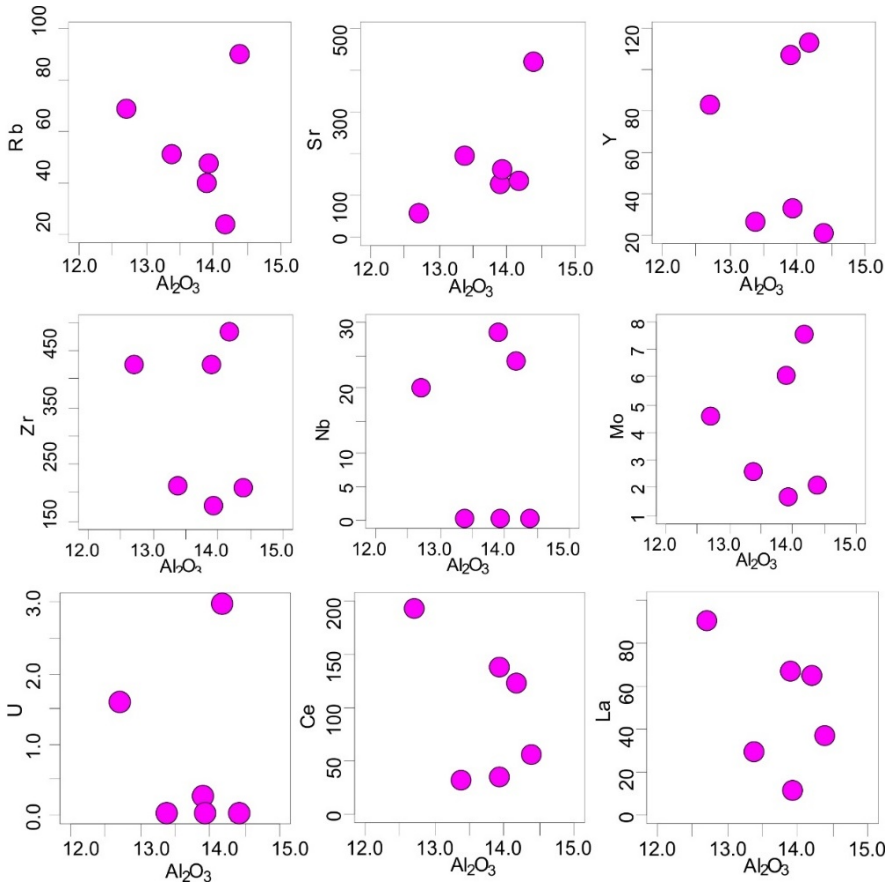

Fig. (8): Multi-elemental variation diagrams of some trace elements (ppm) versus Al2O3 (wt. %) for the studied mélange.

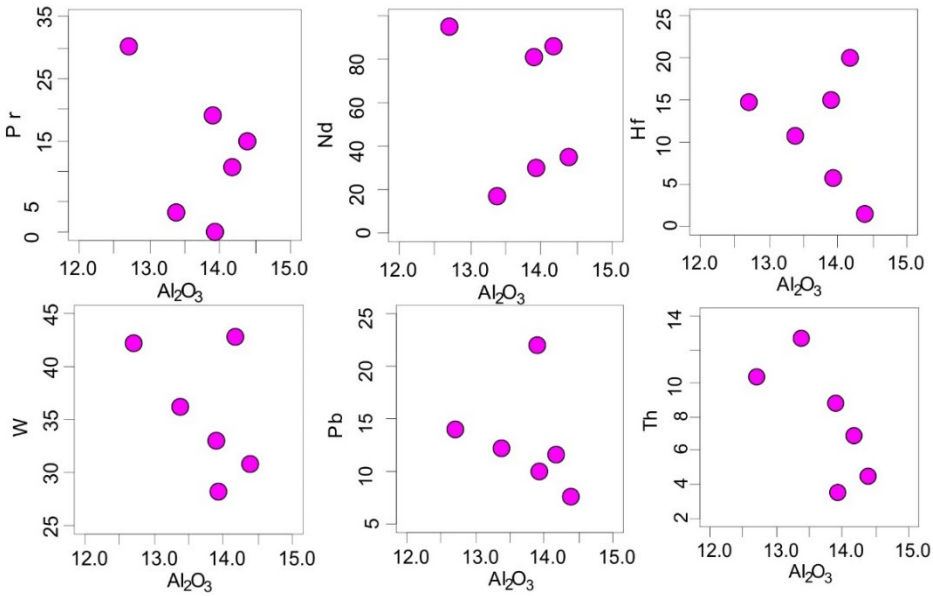

Fig. (9): Multi-elemental variation diagrams of some trace elements (ppm) versus Al2O3 (wt. %) for the studied mélange.

Discussion

Origin of the Protolith

Geochemical analysis suggests a sedimentary origin for the mélange, as evidenced by its position on the P_2O_5/TiO_2 vs. MgO/CaO diagram **(Werner, 1987)** (Fig. 11a). To further constrain the protolith, the mélange's chemical composition was plotted on the log Fe_2O_3/K_2O vs. log SiO_2/Al_2O_3 discrimination diagram

(Herron, 1988). This plot indicates a wacke provenance for most samples, with one sample potentially derived from arkose and another from Fe-shales (Fig. 11b). Furthermore, on the Fe_2O_3 + MgO vs. Na_2O + K_2O diagram of **Blatt et al. (1980)**, which detects sandstone types, the data points fall within the greywacke field (Fig. 11c). The ferrous character of the mélange is further supported by XFe (iron ratio) values ranging from 0.51 to 0.95.

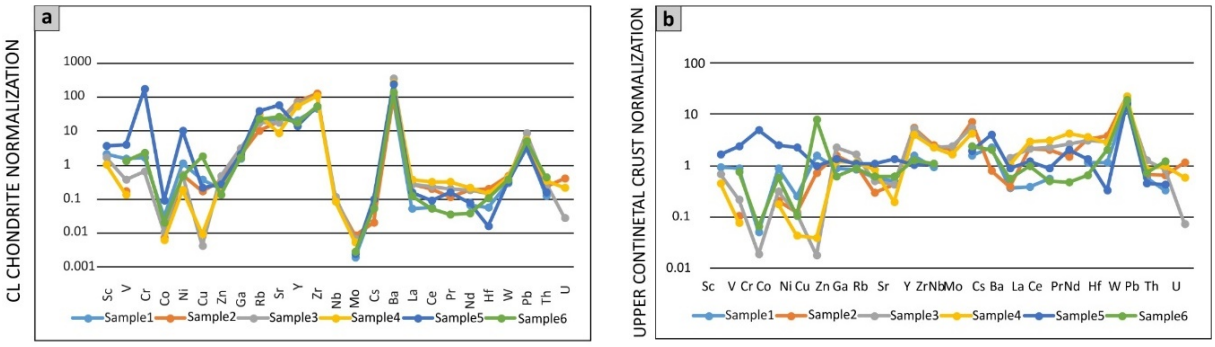

Fig. (10): a) Primitive mantle- and b) upper continental crust-normalized trace element spider diagrams for the studied mélange. Normalization values are from Sun and McDonough (1995) for primitive mantle and Taylor and McLennan (1995) for upper continental crust (UCC).

Chemical Weathering

Geochemical parameters not only characterize the protolith and provenance of meta-sedimentary rocks but also provide insights into the intensity of weathering in the source area. Indices such as the Chemical Index of Alteration (CIA) **(Nesbitt and Young, 1982)**, the Chemical Index of Weathering (CIW) **(Harnois, 1988)**, and the Plagioclase Index of Alteration (PIA) **(Fedo et al., 1995)** are valuable tools for this purpose.

The CIA is calculated as $100[Al_2O_3/(Al_2O_3+CaO^*+Na_2O+K_2O)]$, the CIW as $100[Al_2O_3/(Al_2O_3+CaO+Na_2O)]$, and the PIA as $100[(Al_2O_3 – K_2O)/(Al_2O3+CaO^*+Na_2O-K_2O) \times 1000]$, all expressed in molecular proportions. Unaltered igneous rocks and feldspars typically have CIA values ≤50, while shales exhibit values around 70-75, and residual clays approach 100 **(Nesbitt and Young, 1982, 1984)**. PIA values <60 indicate low chemical weathering, values of 60-80 suggest moderate weathering, and extreme values point to high chemical weathering **(Fedo et al., 1995; Abu El-Enen et al., 2016)**. CIA values for the Sikait-Nugrus-Abu Rusheid mélange range from 54.4 to 92.9, CIW values from 58 to 75, and PIA values from 0.055 to 0.067, indicating low to moderate weathering intensity in the source areas.

Further insights into the maturity of the protolith can be gained from the Index of Compositional Variability (ICV) = $(Fe_2O_3 + K_2O + Na_2O + CaO + MgO + TiO_2)/Al_2O_3$ **(Cox et al., 1995)**. This index measures the abundance of alumina relative to other major cations, reflecting the degree of maturity of mud rocks deposited in a sedimentary basin.

Immature pelitic rocks with a high content of non-argillaceous silicate minerals have ICV values greater than 1, often found in tectonically active settings **(van de Kamp and Leake, 1985)**. Conversely, mature pelitic rocks enriched in clay minerals exhibit low ICV values **(Cox et al., 1995)**, indicating immature protoliths and tectonically active environments where weathering is prevalent **(Weaver, 1989)**.

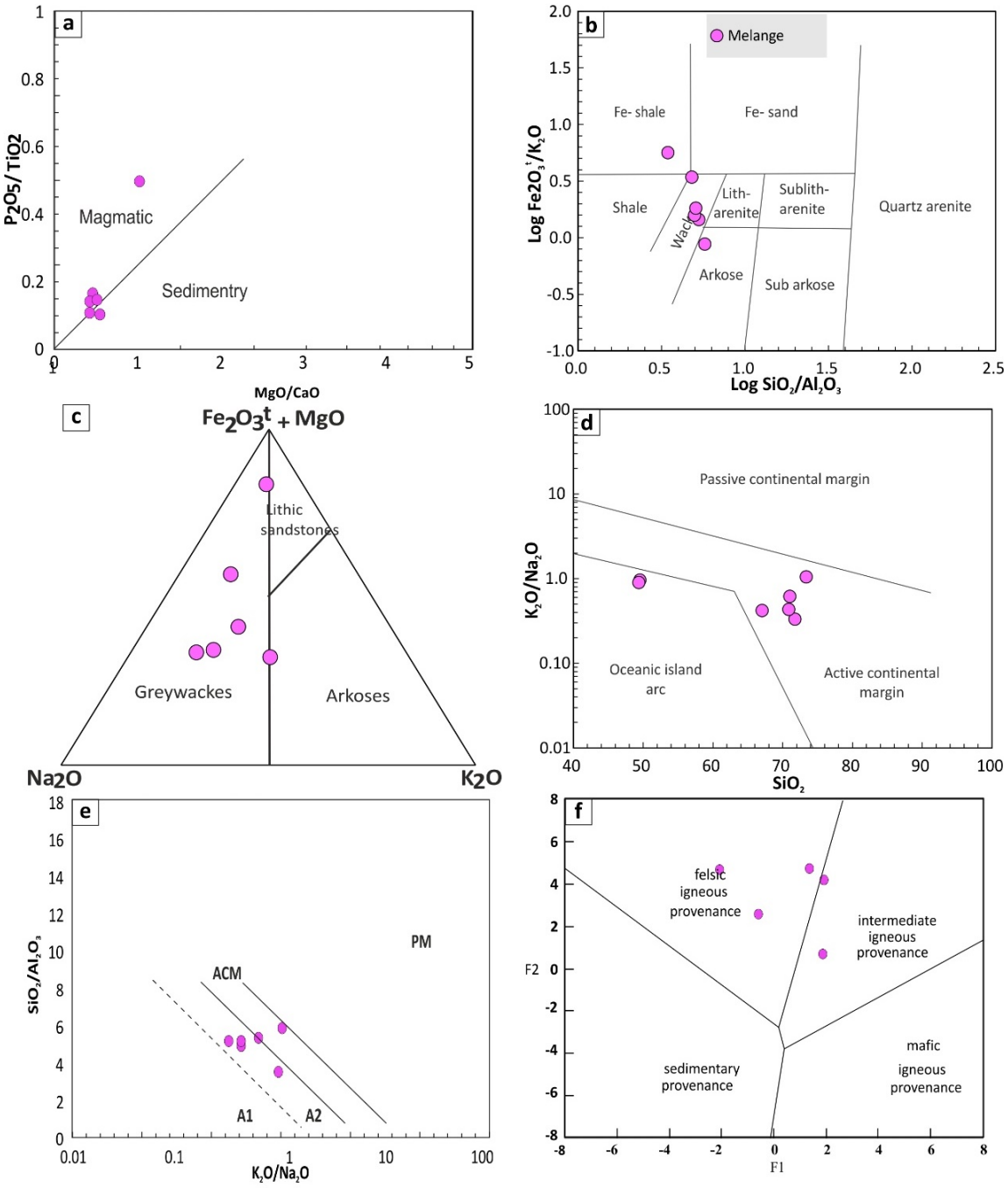

Fig. (11): Geochemical discrimination diagrams for the studied mélange. (a) P_2O_5/TiO_2 vs. MgO/CaO diagram (Werner, 1987). (b) $\log(Fe_2O_3T/K_2O)$ vs. $\log(SiO_2/Al_2O_3)$ diagram (Herron, 1988). (c) $Fe_2O_3(t)$ + MgO vs. Na_2O + K_2O diagram (Blatt et al., 1980). (d) K_2O/Na_2O vs. SiO_2 diagram (Roser and Korsch, 1986). (e) Al_2O_3/Na_2O ratios (Garrels and Mackenzie, 1971). (f) Discriminant function analysis classification plot of function F1 vs. function F2, after Roser and Korsch (1986). $F1 = -1.773TiO_2 + 0.607Al_2O_3 + 0.76Fe_2O_3 - 1.5MgO + 0.616CaO + 0.509Na_2O - 1.224K_2O - 9.09$; $F2 = 0.445TiO_2 + 0.07Al_2O_3 - 0.25Fe_2O_3 - 1.142MgO + 0.438CaO + 1.475Na_2O + 1.426K_2O - 6.86$.

The Sikait-Nugrus-Abu Rusheid mélange displays ICV values ranging from 0.8 to 2.2 (average 1.2), suggesting immature protoliths. This is further supported by Al_2O_3/Na_2O ratios **(Garrels and Mackenzie, 1971)** ranging from 2.5 to 7.6 (average 3.8). The low degree of weathering in the source area and the immaturity of the mélange protolith may be attributed to tectonic activity, as suggested for the Hafafit area by **Stern and Liégeois (2010)**.

Tectonic Setting and Provenance

Geochemical discrimination diagrams provide insights into the tectonic setting of the sedimentary protolith. Using the $Fe_2O_3(t)$+ MgO versus Al_2O_3/SiO_2 diagram proposed by **Bhatia (1983)**, the majority of mélange samples indicate deposition within an active continental margin setting. However, two samples plot within the field indicative of an oceanic island arc tectonic setting (Fig. 11d).

Employing the provenance discrimination diagram of **Roser and Korsch (1988)**, based on major element geochemistry, the mélange samples predominantly cluster within the felsic igneous provenance field, suggesting an acidic igneous protolith. A subset of samples also plots within the intermediate igneous and quartzose sedimentary fields (Fig. 11f).

Collectively, these geochemical parameters suggest that the meta-sedimentary rocks comprising the Sikait-Nugrus-Abu Rusheid mélange experienced low to moderate weathering prior to deposition. The depositional environment is interpreted as either an active continental margin or an oceanic island arc setting. The provenance of these rocks is predominantly felsic igneous, with subordinate contributions from intermediate igneous and quartzose sedimentary sources.

Tectonic Evolution

The complex lithological assemblage and structural relationships observed in the SAN area, combined with the geochemical data, allow for the reconstruction of a multi-stage tectonic history for this segment of the southeastern Hafafit Metamorphic Complex (HMC) within the ANS (Fig. 12). The tectonic evolution of the region can be broadly subdivided into four main stages, reflecting the cyclical nature of tectonic processes in this accretionary orogen:

Stage 1: Initial Accretion and Formation (Island Arc Accretion - D1):

During the early Neoproterozoic (> 620 Ma), the SAN area experienced significant tectonic activity related to the accretion of multiple island arcs onto the eastern margin of the Nile Craton. This accretionary process, driven by northeast-southwest compression, resulted in the formation of the oldest gneisses in the region. The emplacement of ophiolite complexes, now represented by the dismembered ophiolitic blocks within the mélange, also occurred during this stage. Subsequently, a back-arc basin formed behind the newly accreted

island arcs, providing the depositional environment for the immature wackes, Fe-shales, and arkoses that would later become incorporated into the mélange. Tectonic mixing of these sediments with the ophiolitic material (i.e., ultramafic rocks, talc carbonate, talc schist, serpentinite, amphibolite, and metagabbro) led to the formation of the mélange unit itself. This initial stage was characterized by intense deformation, leading to the development of thrust zones and mylonitic fabrics.

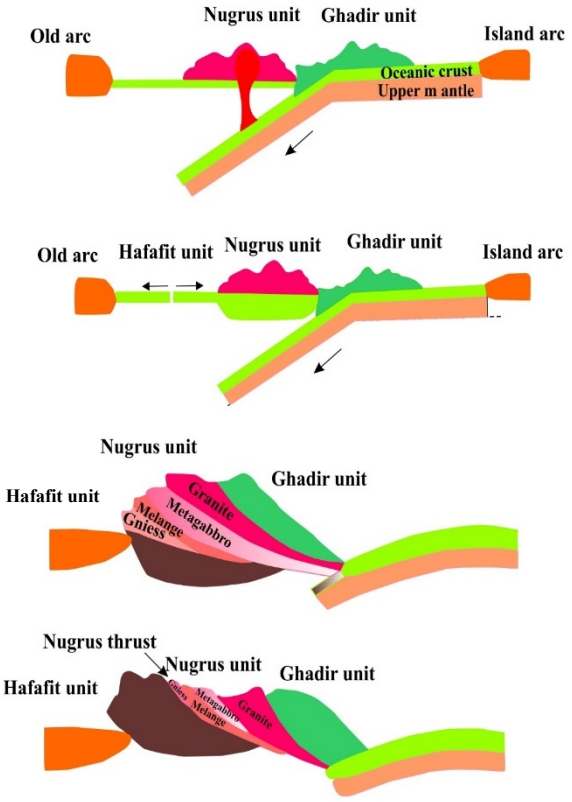

Fig. (12): Schematic illustration of the tectonic evolution of the Sikait-Abu Rusheid-Nugrus area.

Stage 2: Crustal Amalgamation and High-Grade Metamorphism (Obduction and Metamorphism - D2):

Following the initial accretionary phase, renewed compression, related to the collision between East and West Gondwana, culminated in the amalgamation of crustal fragments and the obduction of ophiolites onto the continental margin. This collisional event, peaking at 620-590 Ma, produced high-pressure, high-temperature metamorphism, resulting in the formation of medium- to high-grade metamorphic rocks such as psammitic gneisses, amphibolites, and quartzo-feldspathic gneisses. The prominent Nugrus Thrust, a significant structural boundary in the region, formed during this stage, juxtaposing the ophiolitic mélange against the underlying infrastructural gneisses. These metamorphic rocks preserve evidence of intense deformation, including cataclastic textures and the presence of radioactive minerals such as zircon, thorite, and columbite.

Stage 3: Tectonic Uplift and Shear Zone Development (Extensional Collapse - D3):

Following the peak of collision, the region transitioned into a phase of extensional collapse. This extensional regime led to significant regional uplift, exhumation of deeply buried rocks, and the development of major shear zones, including the prominent, sinistral, thrust-related Nugrus Shear Zone, which facilitated the final emplacement of the mélange unit. The development of complex folding patterns and the intrusion of pegmatite dikes and quartz veins also characterized this stage, further contributing to the structural complexity of the SAN area.

Stage 4: Late-Stage Deformation and Granitoid Intrusion (D4):

The final stage of tectonic evolution in the SAN area underwent additional deformation, including folding, faulting, and the development of shear zones generally trending northeast-southwest and northwest-southeast. This stage also involved the intrusion of various granitoid bodies, including muscovite garnet granite and alkali feldspar granite, often associated with pegmatitic veins. These granitoids exhibit characteristic magmatic textures such as perthitic and myrmekitic intergrowths.

Summary and Conclusion

This study investigated the lithology, geochemistry, and mineralization of the Sikait-Abu Rusheid-Nugrus (SAN) area within the southeastern Hafafit Metamorphic Complex (HMC) of the Arabian-Nubian Shield (ANS). Field observations revealed a diverse assemblage of lithologies, including psammitic gneisses, an ophiolitic mélange, deformed metagabbro, muscovite garnet granite, alkali feldspar granite, and numerous pegmatite dikes and quartz veins.

The psammitic gneisses are subdivided into mineralized and barren types based on their distinct mineralogical characteristics and structural setting. Mineralized gneisses, primarily found in Wadi Abu Rusheid, exhibit a distinctive purple-red coloration and are associated with shearing and the intrusion of granites and pegmatite dikes. These gneisses are often coarse-grained and display augen structures. Barren gneisses, generally lacking distinctive mineralization, are characterized by lighter colors (yellowish-brown to pale pink) and commonly contain enclaves of ophiolitic mélange.

The ophiolitic mélange, a significant unit in the SAN area, is characterized by a schistose matrix hosting blocks of ultramafic rocks (serpentinite, talc-carbonate, talc schist), amphibolite, and metagabbro. The schistose matrix exhibits variations, including garnet-rich schist, amphibolite schist, and quartzo-feldspathic schist. Ultramafic blocks, primarily composed of serpentinite, are also prominent features, ranging in size from small boulders to large blocks.

Petrographic analysis revealed key textural and mineralogical features of each unit, further supporting their field-based classifications. The psammitic gneisses display a well-developed mineral lineation, and a preserved bedding plane (S0) that parallels the metamorphic foliation. Mineralized gneisses are notable for their abundance of radioactive accessory minerals. The ophiolitic mélange exhibits a strong penetrative foliation, often deformed by folds and exhibiting boudinaged pegmatite dikes.

Geochemical analyses of the mélange indicate an origin within an active continental margin setting. The protolith of

the mélange is interpreted to be immature wackes, Fe-shales, and arkoses, deposited in a back-arc basin. These sediments were derived from the erosion of felsic to intermediate igneous source rocks that experienced relatively weak chemical weathering within a tectonically active island arc terrane.

Acknowledgments

The authors express their sincere gratitude to Dr. Tamer Abu-Alam for his insightful discussions and valuable contributions to this research. We thank Prof. Massimo Coltorti, Earth Science Department, Ferrara University, Italy, for major and trace element analyses. We also extend our appreciation to the associate editor and editor for their constructive feedback and editorial efforts in improving this manuscript.

References

Abd El-Naby, H. and Frisch, W., 2006. Geochemical constraints from the Hafafit Metamorphic Complex (HMC): evidence of Neoproterozoic back-arc basin development in the central Eastern Desert of Egypt. *J. Afr. Earth Sci.*, 45(2):173-186.

Abu El-Enen, M. M., Abu-Alam, T. S., Whitehouse, M. J., Ali, K. A., & Okrusch, M., 2016. P–T path and timing of crustal thickening during amalgamation of East and West Gondwana: A case study from the Hafafit Metamorphic Complex, Eastern Desert of Egypt. *Lithos*, 263: 213-238.

Abu-Alam, T.S. and Hamdy, M.M., 2014. Thermodynamic modelling of Sol Hamed serpentinite, South Eastern Desert of Egypt: implication for fluid interaction in the Arabian–Nubian Shield ophiolites. *J. Afr. Earth Sci.*, 99: 7-23.

Abu-Alam, T.S. and Stüwe, K., 2009. Exhumation during oblique transpression: the Feiran–Solaf region, Egypt. *J. Metam, Geol.*, 27(6): 439-459.

Bhatia, M.R., 1983. Plate tectonics and geochemical composition of sandstones. *J. Geol.*, 91(6):611-627.

Blatt, H., Middleton, G. V., and Murray, R. C., 1980. Origin of Sedimentary Rocks. 2nd Ed., Prentice-Hall, New Jersey, 634.

Cox, R., Lowe, D.R. and Cullers, R.L., 1995. The influence of sediment recycling and basement composition on evolution of mudrock chemistry in the southwestern United States. *Geoch., et Cosmoch., Acta*, 59(14): 2919-2940.

El-Ramly, M.F., Greiling, R.O., Rashwan, A.A. and Rasmy, A.H., 1993. Explanatory note to accompany the geological and structural maps of wadi Hafafit Area, Eastern Desert, Egypt. *Ann. Geol. Sur. Egypt*, 9: 1–53.

El-Ramly, M.F., 1984. On tectonic evolution of the Wadi Hafafit area and environs, Eastern Desert of Egypt. *Faculty of Earth Sciences, King Abdulaziz Univ. Bull.*, *6*: 113-126.

El-Bayoumi, R. A., & Greiling, R., 1984. Tectonic evolution of a Pan-African plate margin in Southeastern Egypt—a suture zone overprinted by low angle thrusting. In *Géolo. Afric.,* (pp. 47-56).

El-Gaby, S., List, F.K. and Tehrani, R., 1988. Geology, evolution and metallogenesis of the Pan-African belt in Egypt. In *the Pan-African belt of Northeast Africa and adjacent areas: tectonic evolution and economic aspects of a late proterozoic Oregon* (pp. 17-68).

Fedo, C.M., Wayne Nesbitt, H. and Young, G.M., 1995. Unraveling the effects of potassium metasomatism in sedimentary rocks and paleosols, with implications for paleoweathering conditions and provenance. *Geol.,* 23(10): 921-924.

Fowler, A.R. and El Kalioubi, B., 2002. The Migif–Hafafit gneissic complex of the Egyptian Eastern Desert: fold interference patterns involving multiply deformed

sheath folds. *Tectonophys.*, 346(3-4): 247-275.

Greiling, R.O., Abdeen, M.M., Dardir, A.A., El Akhal, H., El Ramly, M.F., El Din Kamal, G.M., Osman, A.F., Rashwan, A.A., Rice, A.H.N. and Sadek, M.F., 1994. A structural synthesis of the Proterozoic Arabian-Nubian Shield in Egypt. *Geolog., Runds.*, 83: 484-501.

Greiling, R.O., El Ramly, M.F., El Akhal, H. and Stern, R.J., 1988. Tectonic evolution of the northwestern Red Sea margin as related to basement structure. *Tectonophys.*, 153(1-4): 179-191.

Harnois, L., 1988. The CIW index: a new chemical index of weathering. *Sedim., Geol.*, 55(3): 319-322.

Hassanen, M.A., 1997. Post-collision, A-type granites of Homrit Waggat Complex, Egypt: petrological and geochemical constraints on its origin. *Precamb. Res.*, 82(3-4): 211-236.

Herron, M.M., 1988. Geochemical classification of terrigenous sands and shales from core or log data. *J. Sedimentary Res.*, 58(5): 820-829.

Kassem, O.M., Hamimi, Z., Aboelkhair, H., Abdelhalim, A. and Al-Gabali, M., 2019. Microstructural Study and Strain Analysis of Deformed Neoproterozoic Lithologies in the Um Junud Area, Northern Nubian Shield. *Geotecton.,* 53:125-139.

Mackenzie, F.T. and Garrels, R.M., 1971. Evolution of sedimentary rocks (p. 397). New York: Norton.

McDonough, W.F. and Sun, S.S., 1995. The composition of the Earth. *Chem. Geol.*, 120(3-4): 223-253.

Moghadam, H.S., Li, Q.L., Griffin, W.L., Li, X.H., Karsli, O., Spencer, C.J., Santos, J.F., Kirchenbaur, M., Nasir, S. and O'Reilly, S.Y., 2024. Neoproterozoic to early Paleozoic crustal growth, recycling, and the changing geodynamics of North Gondwana. *Gond. Res.*, 126:58-78.

Mohamed, F.H. and Hassanen, M.A., 1997. Geochemistry and petrogenesis of Sikait leucogranite, Egypt: an example of S-type granite in a metapelitic sequence. *Geol. Rund.*, 86:81-92.

Nesbitt, H.W. and Young, G.M., 1984. Prediction of some weathering trends of plutonic and volcanic rocks based on thermodynamic and kinetic considerations. *Geoch., et Cosmoch., acta*, 48(7): 1523-1534.

Nesbitt, H. and Young, G.M., 1982. Early Proterozoic climates and plate motions inferred from major element chemistry of lutites. *nature*, 299(5885): 715-717.

Rashwan, A.A., 1991. Petrography, geochemistry, and petrogenesis of the Migif-Hafafit gneisses at Hafafit Mine area, south Eastern Desert, Egypt, Scientific Series of the International Bureau, 5, Forschungszentrum Julich, p. 359.

Roser, B.P. and Korsch, R.J., 1988. Provenance signatures of sandstone-mudstone suites determined using discriminant function analysis of major-element data. *Chem. Geol.*, 67(1-2):119-139.

Simpson, C. and Wintsch, R.P., 1989. Evidence for deformation-induced K-feldspar replacement by myrmekite. *J. Metam. Geol., 7*(2): 261-275.

Stern, R.J., Ali, K.A., Liégeois, J.P., Johnson, P.R., Kozdroj, W. and Kattan, F.H., 2010. Distribution and Significance of pre-Neoproterozoic Zircons in Juvenile Neoproterozoic Igneous Rocks of the Arabian-Nubian Shield. *Am. J. Sci.,* 310(9): 791-811.

Taylor, S.R. and McLennan, S.M., 1995. The geochemical evolution of the continental crust. *Rev. Geoph.*, 33(2): 241-265.

Van de Kamp, P.C. and Leake, B.E., 1985. Petrography and geochemistry of feldspathic and mafic sediments of the northeastern Pacific margin. *Earth Env. Sci.*

Trans. Royal Soc.Edinburgh, 76(4):411-449.

Weaver, C.E., 1989. *Clays, muds, and shales*. Elsevier.

Werner, C.D., 1987. Saxonian granulites-a contribution to the geochemical diagnosis of original rocks in high-metamorphic complexes. *Gerlands Beitraege zur geophysik*, 96(3-4):271-290.

جيوكيمائية والتطور التكتوني لصخور الميلانج: دراسة لصخور البروتوزويك الحديث في منطقة سكيت – نجرس- أبو رشيد، مصر

ا.د. محمد احمد فؤاد غنيم - ا.د. محمد متولي أبو عنبر- ا.د. عادل محمد حسن – مياده علاء الديب – ا.د. أحمد السعيد إسماعيل مسعود

قسم الجيولوجيا - كلية العلوم - جامعة طنطا

تقع منطقة سيكيت – أبو رشيد – نجرس جنوب مدينة مرسى علم بحوالي 52 كيلومتر، وغرب البحر الأحمر بحوالي 40 كيلومتر. تحدها خطوط العرض 24° 41' 22" - 24° 35' 00" شمالاً، وخطوط الطول 34° 44' 13" - 34° 49' 30" شرقاً.

يتناول هذا البحث دراسة الوضع الجيولوجي والبيئة التكتونية لصخور الميلانج في منطقة سيكيت – أبو رشيد - نجرس - جنوب الصحراء الشرقية - مصر.

تُظهر الدراسات الجيولوجية السابقة، إلى جانب الدراسة الحقلية التفصيلية الحالية، أن منطقة نجرس - سيكيت تحتوي على تتابعات من صخور ما قبل الكمبرى، من الأقدم إلى الأحدث: صخور النايس الرسوبي، صخور الميلانج، الميتاجابرو، صخور الجرانيت، ثم صخور البيجماتيت.

لم تتم دراسة ارتباطات وتطورات هذه الصخور بشكل كافٍ من قبل، نظرًا للتعقيد التكتوني للصخور المختلطة. لذلك، نركز هنا على دراسة المزيج التكتوني (الميلانج) بهدف فهم المصدر التكتوني للخليط من خلال التحاليل الجيوكيميائية الخاصة به. يتكون الميلانج من شست كـmatrix ، وكتل فوق المافية مثل السربنتينيت والشست فوق المافي.

تشير النتائج والدراسات الجيوكيميائية إلى أن الخليط (الميلانج) نشأ في المقام الأول من مصادر نارية مافية، مع بعض العينات المشتقة من الجراى واكى والأركوز مترسبة في حوض القوس الخلفي. وقد تشكل الخليط في البداية خلال الحافة القارية النشطة.

وفرت الدراسة رؤى جديدة حول الجيوكيمياء والتطور التكتوني للخليط في منطقة سيكيت - أبو رشيد - نجرس. يساهم فهم التاريخ التكتوني لهذه المنطقة في فهم أفضل للعمليات التكتونية الأوسع والتطور الجيولوجي للدرع العربي النوبي، ويمكن تلخيصه في النقاط التالية:

1- تراكم جزر القارة (D1): أدى الضغط المبكر (NE-SW) إلى تراكم أقواس الجزر على الحافة الشرقية لقارة (كراتون) النيل، مما أدى إلى تشكيل النيس الأقدم.
2- تكوين حوض القوس الخلفي: ترسيب الرواسب (الجراى واكى والأركوز) في الحوض خلف أقواس الجزيرة. نشأت هذه الرواسب من تجوية أقواس الجزر.
3- الاستقطاب والتحول (D2): أدى اصطدام شرق وغرب جندوانا إلى تحول في الضغط العالي ودرجة الحرارة العالية (الذروة عند 620-590 مليون سنة) وإزاحة الأفيوليت (القشرة المحيطية) على الصخور الموجودة (دفع نجرس).
4- الانهيار الممتد (D3 & D4): رفع المنطقة واستخراجها، بما في ذلك التشوه الهش. قد يكون هذا مرتبطًا بنظام قص الصدوع في نجد.